# Mechanism for anisotropic diffusion of liquid-like Cu atoms in hexagonal $\beta$-$Cu_2S$

Jing Wang [1,*] Keenan Zhuo [1,†] Jianping Gao,[1] Uzi Landman [1] and Mei-Yin Chou [1,2,‡]
[1]*School of Physics, Georgia Institute of Technology, Atlanta, Georgia 30332-0430, USA*
[2]*Institute of Atomic and Molecular Sciences, Academia Sinica, Taipei 106, Taiwan*

(Received 26 October 2020; revised 19 January 2021; accepted 22 June 2021; published 7 July 2021)

$Cu_2S$ in its high-temperature phases is a promising candidate for thermoelectric materials with the combination of a solid S lattice and liquidlike Cu atoms in the context of the so-called phonon-liquid electron-crystal (PLEC) mechanism. The atomic dynamics associated with the high Cu mobility is a critical component in our understanding of the low thermal conductivity in these materials. Among various possible PLEC compounds that have been studied experimentally, hexagonal $\beta$-$Cu_2S$ is a unique case that exhibits anisotropic diffusion channels for Cu atoms in the presence of crystalline S layers. To unveil the diffusion mechanism for such liquidlike Cu atoms, we present first-principles molecular dynamics simulations over 50 ps for hexagonal $Cu_2S$ at 450 K. Quantitative analysis of the atomic radial distributions, mean-square displacements, velocity autocorrelations, and atomic trajectories is reported and confirms the liquid-solid hybrid features. Our simulations reveal the preference of threefold triangular sites by Cu atoms in the S lattice. The triangular sites in the interlayer region do not bind Cu atoms strongly, allowing them to diffuse in the horizontal direction between S layers like a mobile liquid with a calculated diffusion coefficient $\sim 5\times10^{-6}$ $cm^2/s$. The corresponding atomic trajectories have a wide spread and cannot be described by the Chudley-Elliott jump diffusion model. In contrast, Cu atoms are more strongly confined at the triangular sites within the S planes, and Cu diffusion takes place only when the atom hops out of the S layer and enters the interlayer region. This yields a 50% smaller diffusion coefficient in the vertical direction. The anisotropic diffusion channels for liquidlike Cu atoms in hexagonal $\beta$-$Cu_2S$ may provide an additional degree of freedom in designing promising systems for future energy applications.

DOI: 10.1103/PhysRevMaterials.5.073603

## I. INTRODUCTION

Due to the importance of developing energy-related technologies, researchers have made enormous efforts in seeking efficient energy conversion and storage materials. Chalcocite $Cu_2S$ has attracted attention as a viable material in energy applications and has been used, for example, in the electrodes of quantum-dot-sensitized solar cells [1,2], lithium-ion batteries [3,4], sodium-ion batteries [5], and as a light absorber in solar cells [6,7]. In addition, $Cu_2S$ has also been identified as an interesting thermoelectric material that extracts energy out of waste heat by generating electricity from temperature gradients. At high temperatures $\sim$1000 K, the $ZT$ value (the dimensionless thermoelectric figure of merit [8(a)], a criterion to determine the efficiency of thermoelectric materials) of $Cu_{2-x}S$ was reported to be as high as 1.7 experimentally [8(b)]. It was proposed that a major reason for the high $ZT$ value of $Cu_{2-x}S$ is the extremely low thermal conductivity due to disordered, liquidlike Cu atoms, while the crystalline S lattice is responsible for the typical electric conductivity and Seebeck coefficient, an example of the so-called phonon-liquid electron-crystal (PLEC) systems that have been the focus of several recent studies [9–12].

Many previous studies have examined the structure of $Cu_2S$ and made measurements for its structural parameters. $Cu_2S$ has three phases [13–15]: the low-temperature monoclinic phase (low chalcocite or the $\alpha$ phase, existing $<$380 K), the hexagonal phase (high chalcocite or the $\beta$ phase, existing $>$380 K and $<$700 K), and the high-temperature cubic phase (cubic chalcocite or the $\gamma$ phase, existing $>$700 K). The crystal structure of low chalcocite has a monoclinic symmetry (space group $P2_1/c$) with 48 $Cu_2S$ chemical units per unit cell [13]. It is based on a slightly distorted hexagonal close-packed (hcp) framework of S atoms with interstitial Cu atoms mostly surrounded by three S atoms. For the intermediate hexagonal $\beta$ phase, Buerger *et al.* [14] proposed a layered structure stacked along the $c$ axis, as depicted in Fig. 1: the S atoms form an elongated hcp lattice (space group $P6_3/mmc$), and the Cu atoms are randomly distributed with an average of two S and four Cu atoms per unit cell. In contrast, the S atoms in cubic chalcocite form a face-centered cubic lattice (space group $Fm\bar{3}m$) with liquidlike Cu atoms moving around the tetrahedral sites. Recently, Li *et al.* [16] successfully synthesized large hexagonal $Cu_2S$ nanosheets by the supercooling chemical vapor deposition method. The $\alpha$ to $\beta$ phase transition in the 20 $\mu$m nanosheet with a typical thickness of 1.8 nm was found to be at 258 K, 120 K lower than the transition temperature of $\sim$380 K in the bulk, indicating that the $\beta$-phase $Cu_2S$ nanosheet is stable at room temperature.

*fyuyuzaoa@gmail.com
†Present address: Intel Corporation, 2200 Mission College Blvd, Santa Clara, CA 95054, USA.
‡mychou6@gate.sinica.edu.tw

 

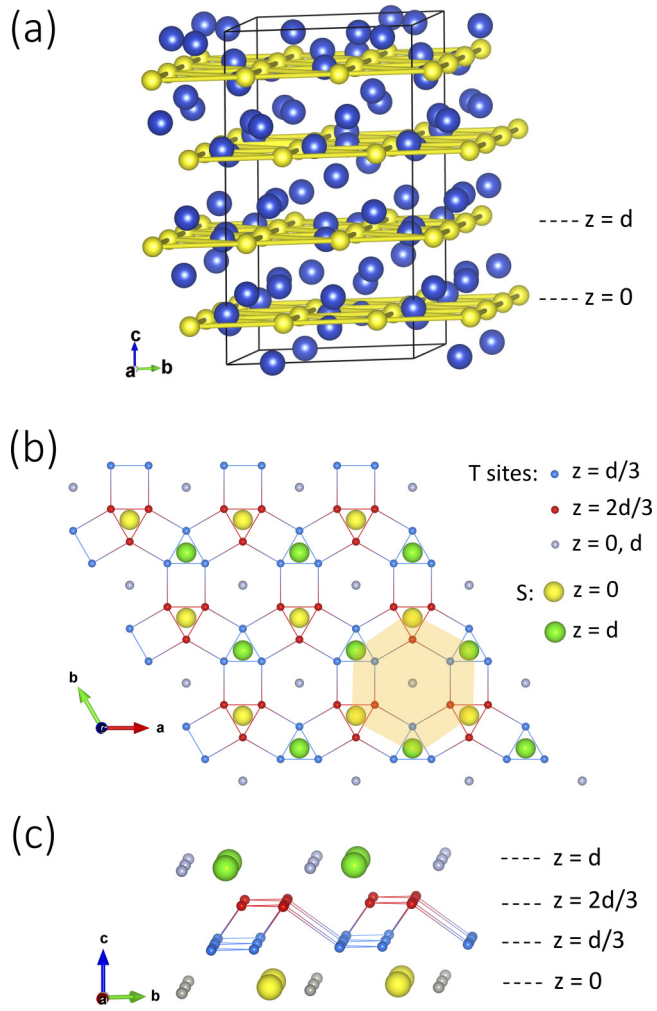


FIG. 1. (a) Structural configuration of a $2 \times 2 \times 2$ unit cell of $\beta$-phase hexagonal $Cu_2S$. The yellow (blue) spheres are S (Cu) atoms. Four horizontal layers of S atoms are shown, with Cu atoms distributed randomly within and between the layers. The package VESTA was used for plotting [26]. (b) Top view and (c) side view showing the geometry of the triangular (T) sites to be occupied by Cu atoms in the S layer and between two adjacent S layers separated by $d$. The interlayer T sites are shown by blue ($z = \frac{1}{3}d$) and red ($z = \frac{2}{3}d$) solid spheres, and the intralayer T sites are shown by gray spheres.

To study the diffusion of Cu atoms in this liquid-solid hybrid system, we have recently performed first-principles molecular dynamics (MD) simulations for cubic $Cu_2S$ and $Cu_2Se$ at 900 K [17]. Exceptionally high Cu diffusion coefficients with values $>10^{-5}$ cm$^2$/s were obtained in the calculation for these weakly ionic compounds, confirming a truly liquidlike behavior like the Cu diffusion property in superionic compounds $Cu_2X$ ($X =$ Cl, Br, or I) [18]. The diffusion mechanism identified through analysis of Cu trajectories was found to be at variance with the commonly used Chudley-Elliott jump diffusion model [19]. Compared with $Cu_2Se$, $Cu_2S$ has an additional hexagonal phase between the high-temperature cubic phase and the low-temperature monoclinic phase. Its hexagonal layered structure presents a unique configuration to investigate direction-dependent diffusion behavior for the Cu atoms. It would also be particularly interesting to examine the diffusion mechanism in this anisotropic system. In a previous first-principles MD study for this hexagonal phase [20], the diffusion coefficient of Cu atoms was found to be $\sim 3.2 \times 10^{-6}$ cm$^2$/s at 450 K, indicating that Cu atoms are almost liquidlike in the hcp lattice formed by S atoms.

Significant Cu mobility is also noted in the low-temperature $\alpha$ phase, giving rise to a variety of interesting phenomena. The transformation between $\alpha$ and $\beta$ phases in $Cu_2S$ nanocrystals was found to occur on a timescale of 20 ps [21] using ultrafast x-ray spectroscopy and scattering techniques, indicating that the transformation is determined by the ionic hopping time. It was also found [22] that solid low-chalcocite nanorods can readily undergo cation exchange and act as catalysts for solution-liquid-solid (SLS)-like growth. Therefore, the combination of the composition conversion and SLS growth can yield a wealth of interesting shapes and morphologies, enabling the creation of tailored heterostructures based on $Cu_2S$ nanostructures [22]. In addition, a unique displacement reaction mechanism was found in the study of $Cu_2S$ nanocrystals reacting with Li, in which Cu metal is extruded from the crystal during the formation of a single $Li_2S$ domain [23]. This results from the reasonably high Cu mobility as well as the similarity of the S sublattices in the initial and final phases, making $Cu_2S$ a promising material for use in rechargeable lithium-ion batteries. Indeed, in electrochemical cells the chemical diffusion coefficients of low chalcocite were found to be in the ranges of $1 \times 10^{-7}$ to $6 \times 10^{-6}$ cm$^2$/s at 60 °C [24] and $1.3 \times 10^{-8}$ to $1 \times 10^{-6}$ cm$^2$/s at 20 °C [25].

In this paper, we present extensive MD simulations of long timescales (>50 ps) and various system sizes with a goal to understand the diffusion mechanism of Cu atoms in $\beta$-phase hexagonal $Cu_2S$. Of particular interest are the characteristics of Cu motion in this superionic compound that exhibits unique anisotropic diffusion channels. Analysis of our simulation data reveals that a Cu atom prefers being surrounded by three S atoms and that two types of triangular (T) sites, intralayer and interlayer, are essential in mapping out the diffusion paths of Cu atoms. The interlayer T sites only weakly confine Cu atoms, so that they move quite freely in the horizontal directions between the S layers. Interestingly, the atomic trajectories have a wide spread in our MD runs and do not support the Chudley-Elliott jump diffusion model for the diffusion direction parallel to the S planes. The calculated diffusion coefficient is $\sim 5 \times 10^{-6}$ cm$^2$/s, confirming the liquidlike feature. In contrast, a Cu atom at an intralayer T site is more strongly bounded, and diffusion only takes place when the Cu atom leaves the S plane by jumping into the region around interlayer T sites. This yields a 50% smaller diffusion coefficient in the direction perpendicular to the S planes. We will also quantitatively analyze the Cu motion data to provide a definitive description of the anisotropic diffusion behavior.

## II. COMPUTATIONAL DETAILS

To better investigate the Cu diffusion pattern in hexagonal $Cu_2S$, we performed long-time first-principles MD simulations within density functional theory. The calculations used the Vienna *Ab initio* Simulation Package (VASP) [27–30] with the projector augmented-wave potentials [31,32] and generalized gradient approximation [33,34]. A 500 eV energy cutoff

was chosen for the plane-wave basis. The equations of motion were integrated using the Verlet algorithm [35], and atomic forces were calculated from the Hellmann-Feynman theorem [36]. All simulations were carried out at 450 K, in the canonical (NVT) ensemble, and with the Nóse-Hoover thermostat [37,38] to control temperature.

The hexagonal unit cell contains four Cu and two S atoms. To check the size effect, we set up the simulation supercells in three different sizes: $(Cu_2S)_{16}$ $(2 \times 2 \times 2)$, $(Cu_2S)_{18}$ $(3 \times 3 \times 1)$, and $(Cu_2S)_{32}$ $(2 \times 2 \times 4)$. The Monkhorst-Pack k-points used were $2 \times 2 \times 2$, $2 \times 2 \times 4$, and $2 \times 2 \times 1$, respectively, for these three simulation cells. The experimental lattice constants $a = 4.03$ Å and $c/a = 1.67$ were used [15], representing a slightly elongated lattice from the ideal $c/a$ ratio of 1.633. We checked the theoretical lattice constants by performing MD runs at 400 K using the $2 \times 2 \times 4$ simulation cell for various $a$ and $c$ values to choose the ones with the lowest absolute value of the average equilibrium pressure (<1 kbar). The results are $a = 4.00$ Å and $c/a = 1.71$, very close to the experimental values.

We first distributed the Cu atoms based on a model proposed previously [39] and performed atomic relaxations to find a low-energy structure for the starting point of MD simulations. The MD simulations were performed on the Born-Oppenheimer surface with a time step of 1 fs. For each system, we began the simulation at 0 K and slowly ramped up the temperature to the desired 450 K over a period of 2 ps. Subsequently, we allowed our systems to equilibrate for at least 10 ps and carefully checked the equilibration condition with longer simulation periods. Then we began collecting data over an additional interval of at least 50 ps, much longer than the simulation time of 12 ps in the previous study [20], at the same temperature of 450 K to have sufficient statistics.

## III. RESULTS AND DISCUSSIONS

### A. Atomic distribution

The liquid-solid hybrid nature and the anisotropic diffusion pattern of Cu atoms in hexagonal $Cu_2S$ are closely connected to its structure. The hexagonal layers of S atoms maintain an hcp crystalline structure, while Cu atoms move in different channels. We first examine the atomic distribution properties obtained in our MD runs. The partial radial distribution function $g_{\alpha\beta}(r)$ measures the probability of finding an atom of species $\beta$ at a distance $r$ from an atom of species $\alpha$. The results from the 50 ps MD run using a $2 \times 2 \times 2$ supercell containing 16 S and 32 Cu atoms are shown in Fig. 2, where comparisons with those from the 0 K solid monoclinic phase are also made. Supercells of all three different sizes yield similar results.

The first peak in each $g_{\alpha\beta}(r)$ gives the most probable separation between species $\alpha$ and $\beta$ based on the simulation data and provides information on the atomic arrangement in the system. From Fig. 2, we find that $g_{SS}(r)$ has very distinct peaks and troughs, indicating an ordered S sublattice. The first peak is at the nearest-neighbor separation $a \approx 4.0$ Å in the hcp lattice, with a full-width-at-half-maximum (FWHM) spread of 0.74 Å at 450 K. The oscillatory behavior in $g_{SS}(r)$ is like that in the 0 K monoclinic phase. Because of the liquid-like nature of Cu atoms, the other partial radial distribution

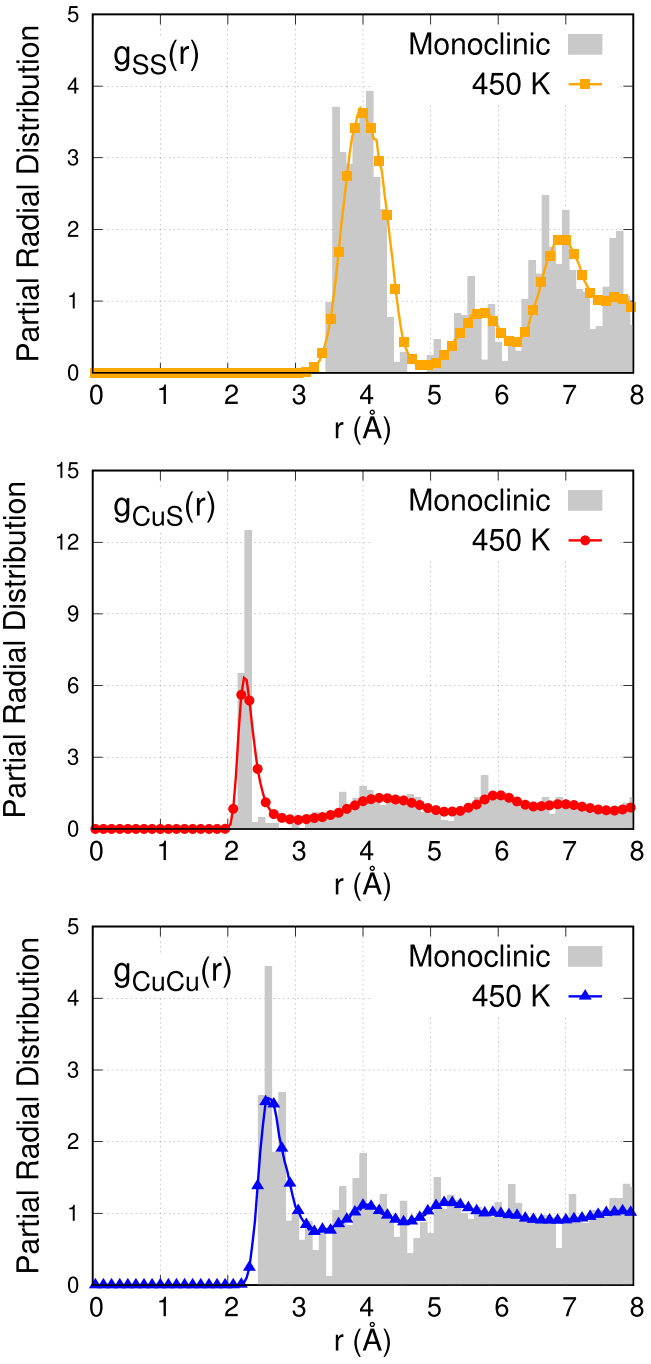


FIG. 2. Partial radial distribution functions obtained from molecular dynamics (MD) simulations of hexagonal $Cu_2S$ at 450 K in comparison with those from the 0 K monoclinic solid phase represented by a histogram with a width of 0.1 Å. The hexagonal phase uses a $2 \times 2 \times 2$ supercell, and the monoclinic phase has a unit cell of $Cu_{96}S_{48}$.

functions $g_{CuS}(r)$, $g_{SCu}(r)$, and $g_{CuCu}(r)$ have a strong first peak, with minor small oscillations at larger distances. The first distinct peak of $g_{CuS}(r)$ $[= g_{SCu}(r)]$ is at about $a/\sqrt{3} \approx 2.3$ Å, indicating that Cu atoms favor T sites surrounded by three nearest-neighbor S atoms. This is consistent with the finding in the previous MD study [20]. The FWHM of the first peak in $g_{CuS}(r)$ is ~0.26 Å, 11% of $a/\sqrt{3}$, indicating a

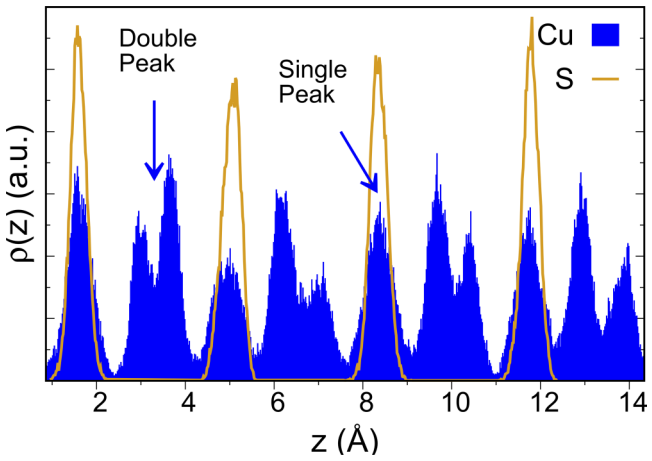


FIG. 3. Number density profiles of hexagonal $Cu_2S$ in the direction perpendicular to the S layers obtained by molecular dynamics (MD) runs at 450 K. The narrow yellow peaks mark the distinct S layers, while the blue profile of Cu atoms exhibits both single peaks (Cu atoms trapped in the S layers) and double peaks (Cu atoms in the interlayer region).

reasonable spread of Cu distribution. In comparison, the 0 K monoclinic phase has several well-defined Cu-S distances.

One can integrate the product of $g_{\alpha\beta}(r)$ and the average number density $\rho_\beta$ of atomic species $\beta$ over the space enclosed by the first minimum of $g_{\alpha\beta}(r)$ to get an estimate of the coordination number $N_{\alpha\beta}$. We obtain $N_{\mathrm{SS}} = 12.0$, consistent with the value for an hcp lattice, and $N_{\mathrm{CuS}} = 3.0$, consistent with the preference for Cu atoms to occupy T sites surrounded by three S atoms. For the hcp S lattice, a triangle can be constructed by including three S atoms in the same layer or two S atoms from one layer and one from the other layer, as shown in Fig. 1(b). The former defines an in-plane (intralayer) T site, and the latter defines an interlayer T site. Each S atom has around it three intralayer and 18 interlayer T sites for Cu atoms to occupy. The value we get for $N_{\mathrm{SCu}}$ is 6.0, indicating that only 28% of these T sites are occupied on average.

Figure 3 shows the atomic density distribution in the $z$ direction (the direction perpendicular to the S planes), calculated from the $2 \times 2 \times 2$ supercell to illustrate the well-defined S layers and meandering Cu atoms. We collect the $z$ coordinates of S and Cu atoms from 5000 evenly distributed snapshots in the 50 ps MD run and then count the population of each discrete $z$ coordinate with a bin width of 0.02 Å to generate the histogram. We could see from the number density profile in Fig. 3 that narrow yellow peaks are the distinct S layers, and Cu atoms in blue have a relatively wider distribution. The small difference in the peak heights at equivalent positions results from the finite statistics in the simulations. About 38% of Cu atoms are in the single peaks coincident with S-layer positions, indicating that they are in the S layers at the intralayer T sites. The other 62% of Cu atoms are in the interlayer region between two adjacent S layers with a double-peak distribution. The two maximal positions in the double peak are $\sim\frac{1}{3}d$ and $\frac{2}{3}d$, corresponding to centers of triangles formed by three S atoms coming from both of the adjacent layers separated by $d$, as shown in Fig. 1(b).

We note that the double peak in the Cu density profile has a large width with an overlapping two-peak structure, indicating that interlayer Cu atoms are not completely confined around the triangular centers and are actually moving around over a large interlayer space. The fact that the single and double peaks are well separated provides a clear identification of two types of Cu atoms: intralayer and interlayer. Diffusion along the $z$ direction will require a conversion between these two types. In Subsec. C, we will examine the diffusion paths by plotting examples of atomic trajectories.

### B. Analysis of atomic diffusion

In self-diffusion systems, calculating the mean square displacement (MSD) from the MD data is a standard practice to evaluate the overall diffusiveness of a specific species $\alpha$:

$$\langle \Delta r_\alpha(t)^2 \rangle = \left\langle \frac{1}{N_\alpha} \sum_{i=1}^{N_\alpha} [\mathbf{r}_i(t) - \mathbf{r}_i(0)]^2 \right\rangle, \tag{1}$$

where $N_\alpha$ is the number of atomic species $\alpha$, and the angle brackets denote the statistical average. To get a reasonably smoothed MSD curve from our 50 ps MD data, we take the statistical average by averaging data over different 40 ps sections of the simulation with origins ($t = 0$) evenly spaced at an interval of 0.5 ps in the first 10 ps. The averaged results from 20 sets of data are shown in Fig. 4. The reason for the choice of 0.5 ps as the time for the origin shift is based on the behavior of the velocity autocorrelation function (VACF) that will be discussed in Subsec. D. One would expect to see a linearly increasing MSD vs time in a diffusive system, and the self-diffusion coefficient $D_{\mathrm{MSD}}$ in a specific direction can be determined by the slope of MSD($t$) [40]:

$$D_{\mathrm{MSD}} = \frac{\partial}{\partial t} \frac{\langle \Delta r^2(t) \rangle}{2N_{\mathrm{dim}}}, \tag{2}$$

where $N_{\mathrm{dim}}$ is the dimension involved.

Figure 4(a) shows the MSD curves for S and Cu atoms in $x$, $y$, and $z$ directions obtained from simulations using a $2 \times 2 \times 2$ supercell. It is clear that there exist different diffusion behaviors for S and Cu atoms. In Fig. 4(a), the MSD curves for S atoms (black lines) in all directions in the 40 ps time period are almost flat at an extremely small magnitude ($<0.15$ Å$^2$), representing confined oscillations around equilibrium positions of a solid lattice. In contrast, the MSD curves for Cu atoms have finite slopes, demonstrating explicit diffusion behavior. We note a considerable difference in the slopes of the curves for in-plane ($x$ and $y$) and perpendicular ($z$) directions. Averaging over results for the in-plane directions, we have $D_\parallel = 4.8 \times 10^{-6}\mathrm{cm}^2/\mathrm{s}$, while the diffusion coefficient for the perpendicular direction is much smaller: $D_\perp = 2.0 \times 10^{-6}\mathrm{cm}^2/\mathrm{s}$. As will be discussed in the next subsection, this anisotropy results from the layered nature of hexagonal $Cu_2S$ in that the Cu atoms can move parallel to the planes in the interlayer region more freely than crossing the S layers. The average diffusion coefficient over all three directions is $D_{\mathrm{Cu}} = 3.8 \times 10^{-6}\mathrm{cm}^2/\mathrm{s}$, close to the value of $3.2 \times 10^{-6}\mathrm{cm}^2/\mathrm{s}$ obtained in a previous study [20].

To evaluate the possible size effect, we have also carried out simulations using two other supercells: $3\times3\times1$ and

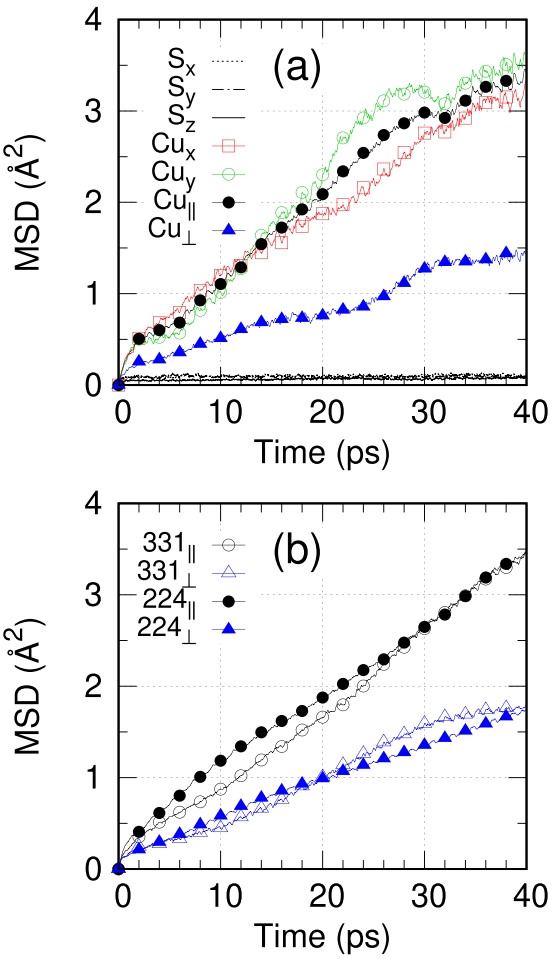


FIG. 4. Atomic mean square displacements (MSDs) in different directions obtained from molecular dynamics (MD) simulations at 450 K: (a) results for both Cu and S atoms using a $2 \times 2 \times 2$ simulation cell, and (b) results for Cu atoms using $3 \times 3 \times 1$ (open symbols) and $2 \times 2 \times 4$ (solid symbols) simulation cells. The dotted/dashed/solid black lines in (a) are results for S atoms, while the MSD curves for Cu atoms are represented by colored symbols. The results for Cu atoms in the parallel direction are averaged values from those of $x$ and $y$ directions.

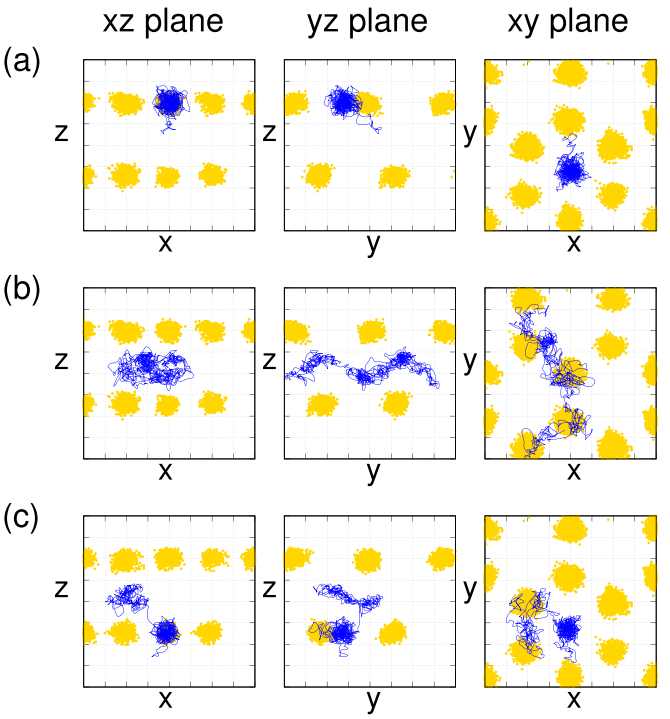


FIG. 5. Atomic trajectories of three representative Cu atoms projected onto the $xz$, $yz$, and $xy$ planes from molecular dynamics (MD) runs at 450 K. Blue lines are the continuous Cu trajectories over a period of 50 ps, and the yellow points are instant positions of S atoms in snapshots taken every 100 fs. The spatial grid interval shown is 1 Å. Trajectories presented are for (a) an intralayer Cu atom, (b) an interlayer Cu atom, and (c) a Cu atoms going through a transition from an intralayer to an interlayer type.

$2\times2\times4$, and the MSD results are shown in Fig. 4(b). The major trend of anisotropic diffusion is found for all sizes of the simulation cells. The final diffusion coefficients are listed and compared in Table I. We find no significant difference in $D_\parallel$, the major part of the Cu diffusion, with increasing the number of S layers. Since the dominant motion occurs in the interlayer region, even the $3\times3\times1$ simulation cell, where a complete set of *AB* stacked S layers are included, gives a reasonably good result within a 5% difference compared with that from the $2\times2\times4$ simulation cell. Surprisingly, the variation of $D_\perp$ values with the cell size in the $z$ direction is also small. This indicates that the size of the simulation cells used in this study is adequate to draw the major conclusions.

### C. Mechanism of Cu diffusion

To identify the diffusion mechanism, we show in Fig. 5 three representative Cu trajectories from MD simulations using a $2 \times 2 \times 2$ supercell. (Supercells of all three different sizes give similar results.) The yellow dots show the positions of S atoms, and the blue lines are Cu trajectories projected onto the $xz$, $yz$, and $xy$ planes. The snapshots are taken every 100 fs in the 50 ps MD simulation. We can see clearly that, even though S atoms move around their equilibrium positions a lot, an hcp lattice is well defined. Three different types of Cu motion are illustrated in Fig. 5 for: (a) a Cu atom largely confined at a T site in the S plane; (b) a Cu atom moving

TABLE I. Diffusion coefficients for Cu atoms in two directions deduced from the MSDs in MD simulations using different supercells.

| Supercell | $D_\parallel (10^{-6}\,cm^2/s)$ | $D_\perp (10^{-6}\,cm^2/s)$ |
|---|---|---|
| $3 \times 3 \times 1$ | 4.3 | 2.5 |
| $2 \times 2 \times 2$ | 4.8 | 2.0 |
| $2 \times 2 \times 4$ | 4.5 | 2.3 |

continuously and randomly in the interlayer region between two S layers; and (c) a mixed-state Cu atom going through a conversion between the intralayer and interlayer characters.

The intralayer Cu atom in Fig. 5(a) moves around a well-defined T site, although the spatial spread is ∼1 Å. The hcp lattice has an *AB* stacking pattern, and we find that intralayer Cu atoms prefer the T sites at the position without S atoms above or below; see the geometry shown in Fig. 1(b). This type of Cu atom can contribute to the diffusion process only if they can move out of the intralayer T sites. However, we find that ∼28% of Cu atoms stay around intralayer T sites during the 50 ps time period, indicating the existence of well-defined potential wells. If we exclude these nondiffusive atoms in the simulation such as the one in Fig. 5(a), the diffusion coefficient calculated in the $2 \times 2 \times 4$ system increases by 22% to $D_{\parallel} = 5.5 \times 10^{-6}\text{cm}^2/\text{s}$ in the in-plane direction.

In contrast, the interlayer Cu atom in Fig. 5(b) moves over a large distance, exhibiting a significant mobility in the horizontal directions. The interlayer T sites have a height of either $\frac{1}{3}d$ or $\frac{2}{3}d$, where $d$ is the interlayer separation. The geometry is shown in Fig. 1(b), where we can see that the interlayer T sites on the same plane ($z = \frac{d}{3}$ or $\frac{2d}{3}$) form a cluster of three with a nearest-neighbor distance of only $\frac{a}{3}$. As shown in Fig. 5(b), interlayer Cu atoms hop through these T sites at $z = \frac{d}{3}$ or $\frac{2d}{3}$ and are confined between two S layers. However, the potential energy landscape seems to be quite flat, so we see continuous trajectories over a wide channel in both the in-plane and vertical directions. The trajectory profile in the $z$ direction is consistent with the double-peak feature in the Cu density plot in Fig. 3, where considerable amplitudes exist between the two peaks at $z = \frac{1}{3}$ and $\frac{2}{3}d$ in the interlayer region.

Figure 5(c) shows the trajectory of a Cu atom that jumps from a confined intralayer site to the interlayer region. Once the conversion is done, the Cu atom gains the typical mobility of an interlayer atom. This indicates that the Cu atom distribution between intralayer and interlayer sites is dynamic and that the exchange of these two types of Cu atoms gives rise to diffusion in the vertical direction, which is therefore expected to be slower than the interlayer diffusion. We note that, in Fig. 5(c), the intralayer and interlayer sections of trajectories are connected by a single line, as seen from both the $xz$ and $yz$ projections. As mentioned previously, the intralayer T sites seem to have relatively deep potential wells, and as a result, the character of the atomic jumps out of these potential wells appears to be consistent with the Chudley-Elliott model [19], where the diffusing atoms reside mostly in these potential wells or in their close vicinity, with occasional swift jumps between the wells. We also remark that some of the diffusion trajectories recorded in our first-principles MD simulations are reminiscent of Lévy flights [41–43]; however, a convincing analysis of the characteristic exponents of the flight-length and flight-time distributions would require longer simulations.

Based on the examination of atomic trajectories, we can conclude that the Cu atom diffusion in the plane is exclusively accomplished by the motion of interlayer Cu between the layers, while the diffusion in the $z$ direction relies on the conversion between intralayer and interlayer Cu atoms. The Cu atoms around the intralayer T sites are more deeply trapped, while the interlayer Cu atoms are much less confined and have a higher mobility. The diffusion models for these two species are therefore quite different.

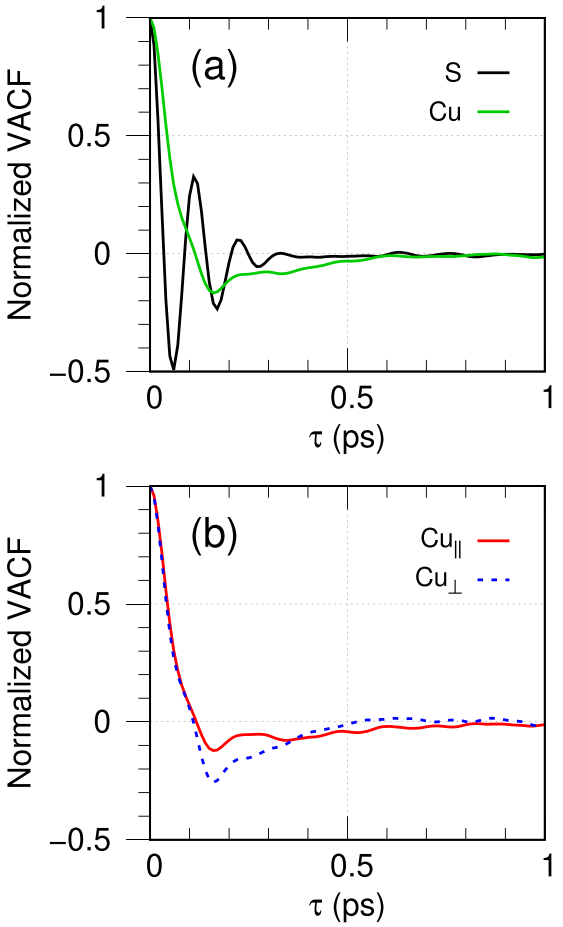


FIG. 6. Velocity autocorrelation functions (VACFs) obtained by molecular dynamics (MD) runs at 450 K using a $2 \times 2 \times 4$ simulation cell. (a) Results for S and Cu atoms averaged over all directions. (b) Results for Cu atoms along two different directions.

### D. VACF and vibrational properties

The VACF provides valuable information on the dynamics of the system. The normalized VACF of a species $\alpha$ is defined as [44]

$$Z_\alpha(\tau) = \frac{\langle \mathbf{v}_i(\tau) \cdot \mathbf{v}_i(0) \rangle}{\langle \mathbf{v}_i(0) \cdot \mathbf{v}_i(0) \rangle}. \quad (3)$$

We have calculated the VACFs for the $2 \times 2 \times 4$ supercell as an example. Figure 6 shows the normalized VACFs of S and Cu atoms, respectively. For both species, the VACF diminishes to almost zero after 0.5 ps, indicating that the time correlation dies out quickly. Therefore, we have used 0.5 ps as the shift of time origin in averaging the MSD results in Subsec. B. In Fig. 6(a), we plot the averaged VACFs for S and Cu atoms. Before damped out after $\tau = 0.4$ ps, the VACF of S atoms exhibits several distinct oscillations as clear evidence of solid lattice behavior. In contrast, the VACF of Cu atoms loses oscillatory peaks and valleys very soon. Compared with the behavior of the VACF for S atoms, this is a strong indication for a more liquidlike motion. Like the

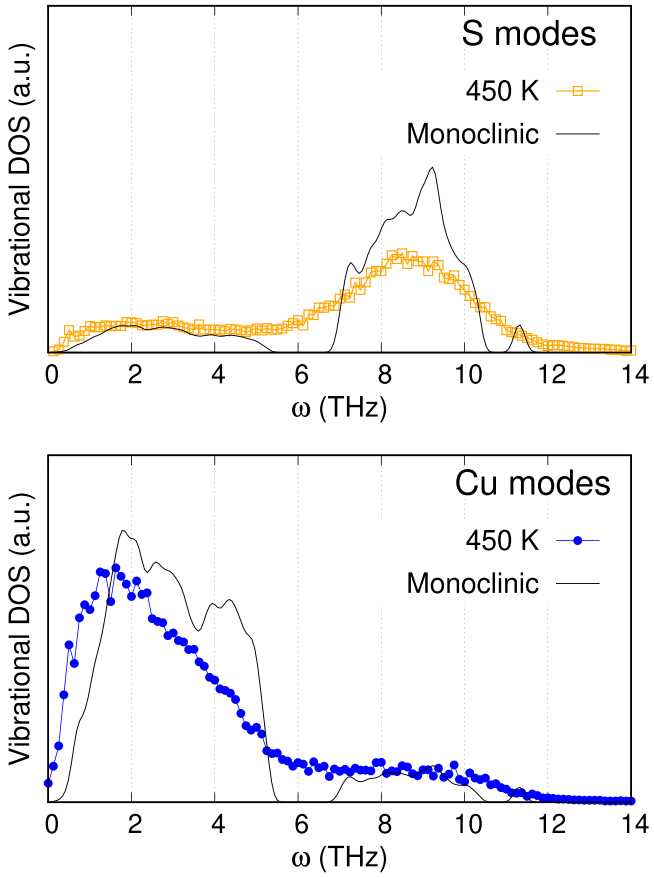


FIG. 7. Comparison of vibrational density of states (DOS) in the hexagonal phase at 450 K obtained by the power spectra and the phonon density states in the monoclinic $Cu_2S$ phase at 0 K. Each curve is properly normalized for comparison.

analysis for the MSD, we separate the VACF for Cu atoms into two directions: parallel and perpendicular to the S planes. The results are plotted in Fig. 6(b). One finds noticeable differences in the magnitude and oscillatory features between the two directions, supporting an anisotropic diffusion of Cu atoms in this hexagonal $Cu_2S$ phase, as concluded by the MSD analysis. A shallower valley is found for the VACF in the direction parallel to the S planes, indicating that Cu atoms lose more structural characters in this direction and thus behave more liquidlike than the motion in the vertical direction.

The vibrational density of states (DOS) is proportional to the power spectrum $\hat{Z}_\alpha(\omega)$, the Fourier transform of the VACF [45]:

$$\hat{Z}_\alpha(\omega) = \frac{1}{\sqrt{2\pi}} \int Z_\alpha(\tau) e^{i\omega\tau} d\tau. \tag{4}$$

We plot in Fig. 7 the calculated vibrational DOS for S and Cu atoms (orange and blue symbols, respectively) for the hexagonal phase at 450 K. The results are compared with the projected phonon DOS of the low-temperature solid monoclinic phase (solid lines) calculated using VASP and the software package PHONOPY [46] for the crystalline unit cell containing 96 Cu atoms and 48 S atoms. A gap of 1.5 THz between the low-energy and high-energy phonon branches is found in the solid monoclinic phase, which is smeared out in the hybrid hexagonal phase. In both systems, we see that the main vibrational peaks of Cu and S are well separated, a special feature that facilitates the partial melting of the Cu atoms as the temperature increases while keeping the S crystalline lattice. The main peak of the S modes is located ∼9 THz in both monoclinic and hexagonal phases, although a clear broadening takes place in the hybrid hexagonal phase, as expected from the more extensive atomic movements. The low-frequency part ($\omega < 5$ THz) exhibits almost no difference in two phases. In comparison, the low-energy Cu modes ($\omega < 6$ THz) show a slight narrowing and a redshift toward the lower energy in the hexagonal phase at 450 K. The curve for Cu has a finite value at $\omega = 0$, an indication that Cu atoms are diffusive compared with S atoms.

A characteristic feature of a simple liquid at rest is that the system cannot sustain a shear stress. Therefore, transverse acoustic (TA) excitation modes normally cannot propagate over long distances in a liquid state. The PLEC model for thermoelectrics performance enhancement is built upon the reduced scattering channels in the liquid part of the system, which leads to a low lattice thermal conductivity and therefore a favorable $ZT$ value. As shown by a recent first-principles MD simulation for layered superionic compound $AgCrSe_2$ [47], the low-energy TA modes of Ag atoms are totally suppressed above the superionic transition temperature when Ag atoms become liquidlike. However, we find a completely different behavior in $Cu_2S$, as shown in Fig. 7. The low-energy part of the vibrational DOS associated with TA Cu motion does not disappear at all at 450 K and even has a redshift, which is not expected for a typical liquid state. This may be explained by the cage effect of preferred triangular sites by Cu atoms as discussed in previous subsections. Experimental evidence of TA excitation modes in liquids was reported by Hosokawa *et al.* [48] using precise dynamic-structure-factor $S(Q, \omega)$ measurements by inelastic x-ray scattering on liquid Ga at 40 °C. They identified weak signatures of low-energy TA excitations in the spectra and explained their existence by instantaneous atomic cages formed in liquid Ga that provide a restoring force for TA modes over short distances. The measured lifetime of these excitations was only ∼0.5 ps. In comparison, the "cage" in our hybrid $Cu_2S$ phase is the triangle formed by crystalline S atoms. This provides a distinct restoring force for the liquidlike Cu atoms and therefore the possibility of sustaining TA vibrational modes, which are expected to be much longer lived.

The redshift in the low-energy Cu modes in Fig. 7 reflects a lower group velocity and is expected to lower the thermal conductivity $\kappa$ since, in classical lattice thermal transport theory, one has $\kappa \propto c v_g l$, where $c$ is the specific heat, $v_g$ is the group velocity, and $l$ is the mean free path. This is consistent with the experimental finding that the thermal conductivity of $Cu_2S$ at 450 K is slightly lower than that of the monoclinic phase below 380 K [8].

## IV. CONCLUSIONS

We have performed long-time first-principles MD simulations at 450 K to study the liquid-solid hybrid phase of hexagonal $\beta$-$Cu_2S$. Three different sizes of the simulation cells are employed and give similar results. Analysis of the

simulation data confirms the liquidlike nature of Cu atoms that exhibit diffusion coefficients $>10^{-6}\,\mathrm{cm}^2/\mathrm{s}$, while the S atoms form an hcp lattice and are not diffusive. The calculated partial radial distribution functions indicate that Cu atoms prefer the triangular sites with three neighboring S atoms. However, the two types of triangular sites, intralayer and interlayer, provide two completely different channels for Cu atom diffusion. The multiple interlayer triangular sites at $z = \frac{1}{3}$ and $\frac{2}{3}d$, where $d$ is the separation between two adjacent S planes, cannot confine Cu atoms effectively, and the MD trajectories show that Cu atoms are quite mobile in the space between the S layers, yielding a high diffusion coefficient $\sim 5 \times 10^{-6}\,\mathrm{cm}^2/\mathrm{s}$ in the direction parallel to the S planes. In contrast, the preferred triangular sites within the S layer are those without S atoms above and below. The simulation trajectories show that they can trap Cu atoms better, and Cu diffusion occurs only when the atom leaves the plane by hopping into a nearby interlayer triangular site. Therefore, the vertical diffusion of Cu atoms has to go through the more confined intralayer triangular sites, yielding a 50% smaller diffusion coefficient. We conclude that $\beta$-$Cu_2S$ has a unique anisotropic diffusion pattern resulting from its two different diffusion channels, and the conversion between interlayer and intralayer characters is essential to facilitate the diffusion process.

We have also examined the vibrational DOS in the liquid-solid hybrid phase by calculating the Fourier transform of the VACF in our simulations and compare the result with the phonon DOS in the low-temperature monoclinic solid phase. The main features of separate Cu and S contributions in different energy ranges are similar in the two phases, with a clear smearing found in the hybrid hexagonal phase as expected. The liquidlike Cu atoms shift the vibrational modes associated with the first peak in the vibrational DOS toward lower energies, which is consistent with the slightly smaller thermal conductivity in the hybrid phase. The overall features of the vibrational spectra do not change much in the hybrid phase due to similar local geometry since the mobile Cu atoms still show the preference of being surrounded by three S atoms.

## ACKNOWLEDGMENTS

M.-Y.C. acknowledges support from Academia Sinica under Grant No. AS-SS-109-01, and U.L. acknowledges support from the Air Force Office of Scientific Research (AFOSR), Grant No. FA9550-21-1-0198. This paper used resources of the National Energy Research Scientific Computing Center (NERSC), a U.S. Department of Energy Office of Science User Facility operated under Contract No. DE-AC02-05CH11231.

[1] J. G. Radich, R. Dwyer, and P. V. Kamat, J. Phys. Chem. Lett. **2**, 2453 (2011).
[2] Y. Jiang, X. Zhang, Q.-Q. Ge, B.-B. Yu, Y.-G. Zou, W.-J. Jiang, W.-G. Song, L.-J. Wan, and J.-S. Hu, Nano Lett. **14**, 365 (2013).
[3] B. Jache, B. Mogwitz, F. Klein, and P. Adelhelm, J. Power Sources **247**, 703 (2014).
[4] X. Rui, H. Tan, and Q. Yan, Nanoscale **6**, 9889 (2014).
[5] Q. Li, Q. Wei, Q. An, L. Huang, W. Luo, X. Ren, K. A. Owusu, F. Dong, L. Li, P. Zhou, L. Mai, Q. Zhang, K. Amine, and J. Lu, Energy Storage Mater. **16**, 625 (2019).
[6] C. Pan, S. Niu, Y. Ding, L. Dong, R. Yu, Y. Liu, G. Zhu, and Z. L. Wang, Nano Lett. **12**, 3302 (2012).
[7] Y. Zhao and C. Burda, Energy Environ. Sci. **5**, 5564 (2012).
[8] (a) In the figure of merit, ZT, the parameter Z is the square of the Seebeck voltage per unit of temperature, multiplied by the electrical conductivity and divided by the thermal conductivity, and T is the absolute temperature; for reviews see, L. E. Bell, Science **321**, 1457 (2008) and G. J. Snyder and E. S. Toberer, Nat. Mater. **7**, 105 (2008); (b) Y. He, T. Day, T. Zhang, H. Liu, X. Shi, L. Chen, and G. J. Snyder, Adv. Mater. **26**, 3974 (2014).
[9] J. L. Niedziela, D. Bansal, A. F. May, J. Ding, T. Lanigan-Atkins, G. Ehlers, D. L. Abernathy, A. Said, and O. Delaire, Nat. Phys. **15**, 73 (2019).
[10] J. Ding, J. L. Niedziela, D. Bansal, J. Wang, X. He, A. F. May, G. Ehlers, D. L. Abernathy, A. Said, A. Alatas, Y. Ren, G. Arya, and O. Delaire, Proc. Natl. Acad. Sci. U.S.A. **117**, 3930 (2020).
[11] K. Zhao, A. B. Blichfeld, E. Eikeland, P. Qiu, D. Ren, B. B. Iversen, X. Shi, and L. Chen, J. Mater. Chem. **5**, 18148 (2017).
[12] K. S. Weldert, W. G. Zeier, T. W. Day, M. Panthoöfer, G. J. Snyder, and W. Tremel, J. Am. Chem. Soc. **136**, 12035 (2014).
[13] H. T. Evans, Z. Kristallogr. Cryst. Mater. **150**, 299 (1979).
[14] M. Buerger and B. J. Wuensch, Science **141**, 276 (1963).
[15] G. Will, E. Hinze, and A. R. M. Abdelrahman, Eur. J. Mineral. **14**, 591 (2002).
[16] B. Li, L. Huang, G. Zhao, Z. Wei, H. Dong, W. Hu, L.-W. Wang, and J. Li, Adv. Mater. **28**, 8271 (2016).
[17] K. Zhuo, J. Wang, J. Gao, U. Landman, and M.-Y. Chou, Phys. Rev. B **102**, 064201 (2020).
[18] J. X. Zheng-Johansson, K. Sköld, and J.-E. Jørgensen, Solid State Ionics **70**, 522 (1994).
[19] C. Chudley and R. Elliott, Proc. Phys. Soc. **77**, 353 (1961).
[20] L.-W. Wang, Phys. Rev. Lett. **108**, 085703 (2012).
[21] T. Miller, J. Wittenberg, H. Wen, S. Connor, Y. Cui, and A. Lindenberg, Nat. Commun. **4**, 1369 (2013).
[22] Y. Zhai and M. Shim, ChemPhysChem **17**, 741 (2016).
[23] M. T. McDowell, Z. Lu, K. J. Koski, J. H. Yu, G. Zheng, and Y. Cui, Nano Lett. **15**, 1264 (2015).
[24] H. Rickert and H.-D. Wiemhöfer, Solid State Ionics **11**, 257 (1983).
[25] U. Tinter and H.-D. Wiemhöfer, Solid State Ionics **9**, 1213 (1983).
[26] K. Momma and F. Izumi, J. Appl. Crystallogr. **44**, 1272 (2011).
[27] G. Kresse and J. Hafner, Phys. Rev. B **47**, 558 (1993).
[28] G. Kresse and J. Hafner, Phys. Rev. B **49**, 14251 (1994).
[29] G. Kresse and J. Furthmüller, Comput. Mater. Sci. **6**, 15 (1996).
[30] G. Kresse and J. Furthmüller, Phys. Rev. B **54**, 11169 (1996).
[31] P. E. Blöchl, Phys. Rev. B **50**, 17953 (1994).
[32] G. Kresse and D. Joubert, Phys. Rev. B **59**, 1758 (1999).

[33] J. P. Perdew, J. A. Chevary, S. H. Vosko, K. A. Jackson, M. R. Pederson, D. J. Singh, and C. Fiolhais, Phys. Rev. B **46**, 6671 (1992).
[34] J. P. Perdew, J. A. Chevary, S. H. Vosko, K. A. Jackson, M. R. Pederson, D. J. Singh, and C. Fiolhais, Phys. Rev. B **48**, 4978(E) (1993).
[35] L. Verlet, Phys. Rev. **159**, 98 (1967).
[36] R. P. Feynman, Phys. Rev. **56**, 340 (1939).
[37] S. Nosé, J. Chem. Phys. **81**, 511 (1984).
[38] W. G. Hoover, Phys. Rev. A **31**, 1695 (1985).
[39] P. Lukashev, W. R. L. Lambrecht, T. Kotani, and M. van Schilfgaarde, Phys. Rev. B **76**, 195202 (2007).
[40] D. Frenkel and B. Smit, *Understanding Molecular Simulation* (Academic Press, Orlando, FL, 1996).
[41] M. F. Shlesinger, G. M. Zaslavsky, and U. Frisch (eds.), *Lévy Flights and Related Topics in Physics* (Springer, Berlin, 1995).
[42] J.-P. Bouchaud and A. Georges, Phys. Rep. **195**, 127 (1990).
[43] W. D. Luedtke and U. Landman, Phys. Rev. Lett. **82**, 3835 (1999).
[44] A. M. Ovrutsky, A. S. Prokhoda, and M. S. Rasshchupkyna, *Computational Materials Science: Surfaces, Interfaces, Crystallization* (Elsevier, Amsterdam, 2013).
[45] J. P. Hansen and I. R. McDonald, *Theory of Simple Liquids* (Academic Press, London, 2013).
[46] A. Togo and I. Tanaka, Scr. Mater. **108**, 1 (2015).
[47] C. Wang and Y. Chen, npj Comput. Mater. **6**, 26 (2020).
[48] S. Hosokawa, M. Inui, Y. Kajihara, K. Matsuda, T. Ichitsubo, W.-C. Pilgrim, H. Sinn, L. E. González, D. J. González, S. Tsutsui, and A. Q. R. Baron, Phys. Rev. Lett. **102**, 105502 (2009).